PROC. OF JSCE,
No. 200, APRIL 1972

SHOCK TUBE STUDY ON STRESS WAVE PROPAGATION IN CONFINED SOILS

By Koichi AKAI, Masayuki HORI**, Nobuo ANDO*** and Tamio SHIMOGAMI****

1. INTRODUCTION

Research on the one-dimensional propagation of stress wave through soil has a meaningful significance in the study of wave characteristics in their propagation process from the seismic source to the ground surface and in investigating the dynamic behavior of soils including wave effect due to rapid loadings.

In the conventional stress propagation test, the pulsative type pressure was obtained by hitting an end of rod specimens by another materials and the propagating stress in the rod was picked up[1),2)]. Such procedures are rather primitive, however, because we obtain neither a surface pressure with uniform wave form nor a controlled stress. On the other hand, one can produce a uniform wave with a distinct shock front by means of shock tube. The history of shock tube is very old and the theory has been sufficiently systemalized in the field of aerodynamics. It is easy to calculate the magnitude and the form of shock wave by this technique theoretically, as well as their adjustment in practice. The authors attempt to build up this type of apparatus as the loading device to the surface of confined soil, and to increase the precision of stress propagation test.

2. DESIGN OF SHOCK TUBE

(1) General

In 1899 Vieille used a shock tube, 22 mm in diameter and 6 m long, for the first time in France. Collodion, paper, glass and steel foil were used as diaphragms in the shock tube[3)]. After that, shock tube was not used much. Since 1940, however, the utilities of shock tube have been noticed and it is being used throughout in many branches of science. It is used not only in the field of supersonic aerodynamics, but also in chemistry in order to solve dynamic problems for the mixture of gases in very high pressure. Also, it is used to examine the dynamic properties of soils using a regular wave form obtained from the shock tube[4),5)].

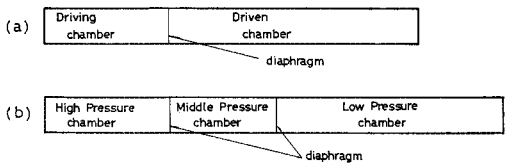

Fig. 1 Shock tube with (a) two chambers and (b) three chambers.

There are two kinds of shock tube. One is shown in Fig. 1(a). It consists of two chambers, a high pressure cell called the driving chamber and a low pressure cell called the driven chamber separated by a thin diaphragm. The other one (Fig. 1(b)) has three chambers, containing high, middle and low pressures, respectively, by which higher shock pressure can be obtained. Applying required pressure to the gases in these chambers and then breaking the diaphragms by a suitable method, a shock wave with sharp wave front propagates through the low pressure chamber.

The advantages in utilizing the latter type of shock tube as a loading apparatus on confined soils to determine the dynamic properties of soils are:

1) It is easy to control the magnitude of a shock pressure.
2) Wave form of shock pressure obtained has a sharp wave front for which the analysis can be easily performed.

* Dr. Eng., Professor of Civil Engineering, Kyoto University.
** M.S.C.E., Doctorial course student, Kyoto University.
*** Postgraduate, Kyoto University.

(2) Theory of Shock Tube

Let us consider a shock tube with a constant cross sectional area. The typical type of tube is shown in Fig. 2(a). In Fig. 2(b), 1 indicates the

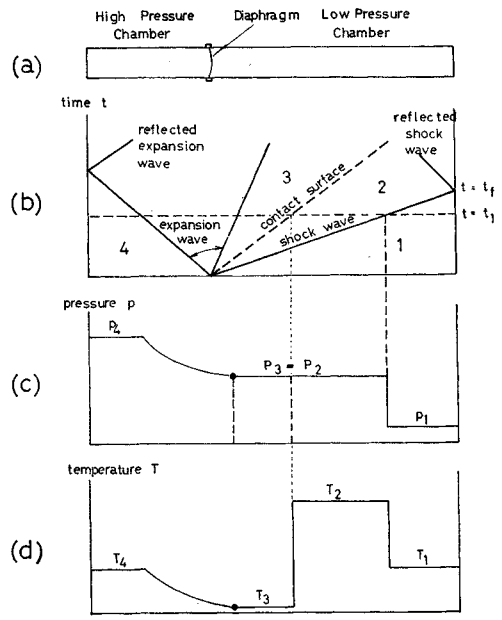

Fig. 2 Shock tube; (a) typical type of tube, (b) schematic diagram of shock wave and expansion wave, (c) distribution of pressure and (d) distribution of temperature.

region where the shock wave does not arrive in, 2 the region between the shock wave and the contact surface, 3 the region between the contact surface and the expansion wave, and 4 the region where the expansion wave does not arrive in. Figs. 2(c) and (d) show the distribution of pressure and temperature, respectively, along the tube axis at any time t_1 ($t_1<t_f$) after the diaphragm is broken off.

It is assumed that a perfect gas is used in the

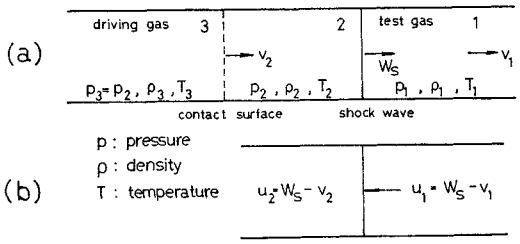

Fig. 3 State of gas in a tube; (a) from outside and (b) on the shock wave.

tube. Fig. 3 shows the state of gas in the tube; (a) the state which an observer outside the tube can see and (b) one which an observer on the shock wave can see. If we take the latter situation, the relative velocities of gas flows in the front and the rear of the shock wave are, respectively:

$$u_1=w_s-v_1\,,\quad u_2=w_s-v_2 \qquad \cdots\cdots(1)$$

where, w_s denotes the progressive velocity of shock wave, v_1 and v_2 the velocities of gases in the region 1 and 2, respectively ($v_1=0$ in the tube). Applying the conservation laws of mass, momentum and energy at the wave front in two regions 1 and 2, we find[6]

$$\rho_1 u_1=\rho_2 u_2 \qquad \cdots\cdots(2)$$

$$p_1+\rho_1 u_1^2=p_2+\rho_2 u_2^2 \qquad \cdots\cdots(3)$$

$$h_1+\frac{1}{2}u_1^2=h_2+\frac{1}{2}u_2^2 \qquad \cdots\cdots(4)$$

where, h_1 and h_2 are the enthalpies per unit mass of gas in the front and the rear of the shock wave, respectively. Under the assumption of the perfect gas we obtain the following correlations:

$$h=c_pT\,,\quad \gamma=c_p/c_v \qquad \cdots\cdots(5)$$

where, T denotes the absolute temperature, c_p and c_v the specific heats at constant pressure and constant volume, respectively, and γ the specific heat ratio.

By combining Eqs. (2), (3), (4) and (5), we obtain

$$\frac{p_2}{p_1}=\frac{1-\dfrac{\gamma-1}{\gamma+1}\dfrac{\rho_1}{\rho_2}}{\dfrac{\rho_1}{\rho_2}-\dfrac{\gamma-1}{\gamma+1}} \qquad \cdots\cdots(6)$$

This equation is well known as Rankine-Hugoniot's equation. It is conventional to represent the intensity of a shock wave in tube by the shock Mach number which is defined by

$$M_1=\frac{W_s}{a_1} \qquad \cdots\cdots(7)$$

where, a_1 is the acoustic velocity in the region 1. After performing some reductions we obtain the following equation with Mach number instead of Eq. (6).

$$\frac{p_2}{p_1}=\frac{2\gamma_1 M_1^2-(\gamma_1-1)}{\gamma_1+1} \qquad \cdots\cdots(8)$$

Moreover, the relationship between the ratio of initial pressures (p_4/p_1) and shock Mach number is given by

$$\frac{p_4}{p_1}=\frac{2\gamma_1 M_1^2-(\gamma_1-1)}{\gamma_1+1}\times\left\{1-\frac{\gamma_4-1}{\gamma_1+1}\frac{a_1}{a_4}\left(M_1-\frac{1}{M_1}\right)\right\}^{-2\gamma_4/(\gamma_4-1)} \qquad \cdots\cdots(9)$$

This relationship indicates that, if p_1 and p_4 are known, the intensity of shock wave in the low pressure chamber depends on the specific heat ratios, γ_1 and γ_4, and the acoustic velocity of the gas in the high pressure chamber.

A shock wave reaching the end of low pressure chamber is reflected backward. When the gas pressure is measured at the end of the tube, therefore, it is the sum of the pressure of incident and reflected shock wave. Denoting p_5 as the pressure due to the reflected shock wave, the ratio p_5/p_1 is given by

$$\frac{p_5}{p_1}=\left\{\frac{2\gamma_1 M_1^2-(\gamma_1-1)}{\gamma_1+1}\right\}\left\{\frac{(3\gamma_1-1)M_1^2-2(\gamma_1-1)}{(\gamma_1-1)M_1^2+2}\right\} \quad \cdots\cdots(10)$$

As long as the gas in the high pressure chamber is expanding, a shock wave is maintained. When the pressure in the high pressure chamber decreases below that of the wave in the tube, the shock wave vanishes. When the expansion wave reflected at the end of high pressure chamber catches up the contact surface and the reflected shock wave, the shock wave gradually attenuates. The point at which these phenomena take place depends on the initial condition and the size of the tube used.

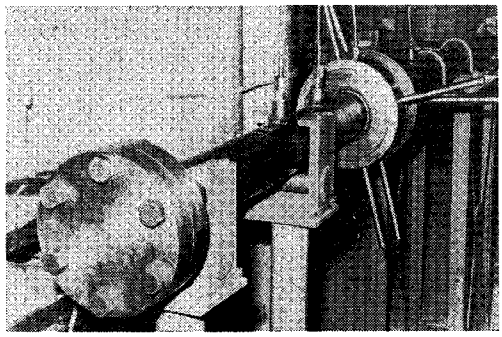

Photo. 1 Shock tube.

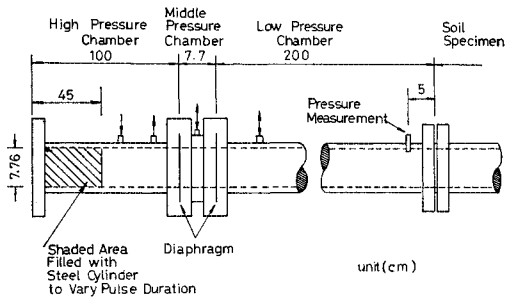

Fig. 4 Schematic diagram of the shock tube used.

(3) Use of Shock Tube

The schematic diagram of the shock tube used in the present study (Photo. 1) is shown in Fig. 4. It consists of high pressure chamber, middle pressure chamber and low pressure chamber. All chambers are made of cylindrical steel tube with the inside diameter of 7.76 cm and 1.2 cm in thickness. In general, it is said that if the length of low pressure chamber is more than ten times the inside diameter, a uniform shock wave can be obtained at the end of tube. Since a 2 m-long low pressure chamber is used in this study, *i.e.*, the ratio of them is twenty six, therefore, sufficiently uniform shock wave will be obtained. At the distance of 5 cm from the end of tube, a semi-conductor type pressure transducer is equipped in order to measure the shock pressure. In the experiment of stress wave propagation in soils, a steel chamber to confine the soil specimen is connected with the shock tube as shown in the figure. The description of soil specimens will be given later in detail.

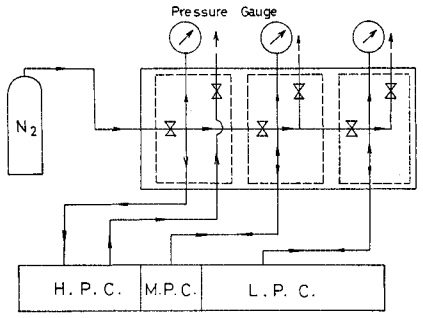

Fig. 5 Schematic diagram of the gas controlling system.

Fig. 5 is a schematic diagram of the gas controlling system. In experiments the low pressure chamber is atmospheric, while compressed nitrogen gas is used for the high and middle pressure chambers. Two disks of thin aluminium with 17.5 cm in diameter are used as the diaphragms to separate the high, middle and low pressure chambers. By using similar diaphragms Kamimoto presented the following empirical relationship between the rupture pressure and the thickness of them[7]:

$$\frac{p_R/\sigma_t}{t/d}=4.40\sim3.80 \quad \text{(average 4.0)}\cdots\cdots(11)$$

where, p_R denotes the pressure at rupture, σ_t the tensile stress intensity of the material used, t the thickness and d the diameter of cross section

subjected to pressure. The correlation between the rupture pressure and the thickness of the diaphragms obtained by the present experiment is shown in Fig. 6. The solid line in this figure is obtained from Eq. (11). In this case, σ_t=1 000 kg/cm^2 and d=7.76 cm are used.

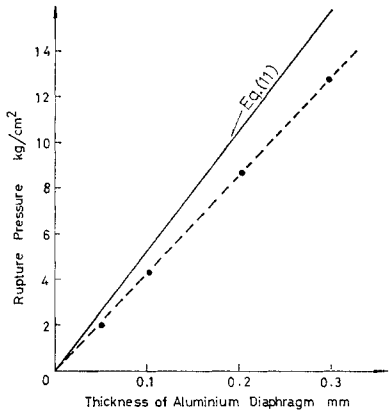

Fig. 6 Correlation between the rupture pressure and the thickness of diaphragms.

The operations of this shock tube are as follows:

1) We set up two diaphragms with an appropriate thickness that they do not rupture during the operation 2) and do rupture by the operation 3).
2) We apply pressures into the middle and high pressure chambers at the same time and stop applying them, at the instant when they become half of the required pressure for the high pressure chamber. Then, we apply pressure only into the high pressure chamber till the required value is reached.
3) We exhaust the gas in the middle pressure chamber suddenly. By this operation, two diaphragms rupture instantaneously and the shock wave propagates into the low pressure chamber.

In order to know experimentally the relationship between initial pressure in the high pressure chamber and obtained shock pressure, the above operations are carried out by covering the end of tube with a steel plate. The typical wave form picked up by the pressure transducer at the end of tube is shown in Photo. 2(a). Such wave form is termed the cushioned impact by Whitman[8]. Also we can see in Photo. 2(b) that the shock wave reflects so many times at the both ends of the tube. In the present study the authors deal only with the first shock pressure.

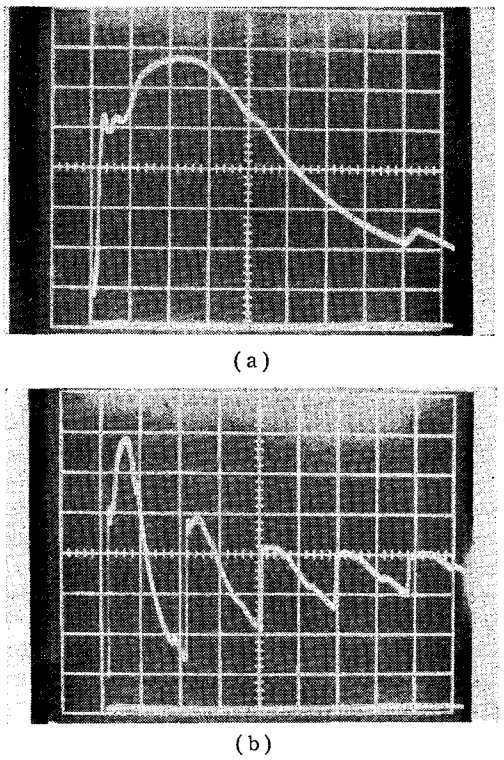

(a)

(b)

Photo. 2 (a) Typical wave form (sweep: 2 msec/cm) and (b) reflected shock waves (sweep: 10 msec/cm).

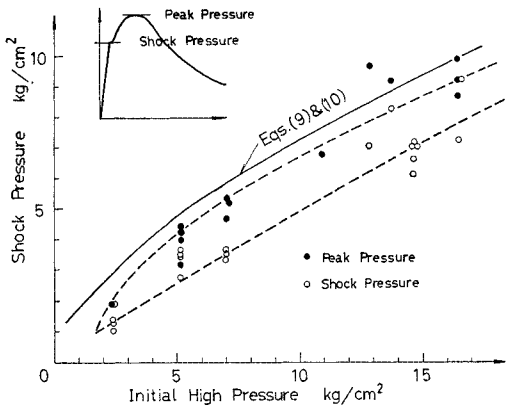

Fig. 7 Relationship between the initial pressure and the obtained shock pressure.

The relationship between the initial pressure and the obtained shock pressure is summarized in Fig. 7. The solid line in the figure is the theoretical curve obtained from Eqs. (9) and (10), where the specific heat ratio γ_1(air)=γ_2(N_2)=1.404 and the acoustic velocity ratio a_1/a_4=1.0 are adopted in this case.

3. EXPERIMENTS

(1) Apparatus and Procedure

a) Design of Apparatus

A testing apparatus for one-dimensional stress wave propagation was designed to confine soil specimens as shown in Fig. 8(a). This confining tube was horizontally connected with the shock tube. This was made of steel with an inside diameter of 7.6 cm, wall thickness of 6.5 mm and 2 m long. It is long enough to neglect the influence of a reflected stress wave at the reflection end of the tube, marked as R in the figure.

The cross section of the tube is perfect circular as shown in Fig. 8(b). In putting the soil column in the tube, one can take off the upper half of it (A). The upper half of the tube consists of five segments. As shown in Fig. 8(c), each segment is 40 cm long and has splits at the both ends through which we can take out leads from various measuring devices embedded in the soil specimen.

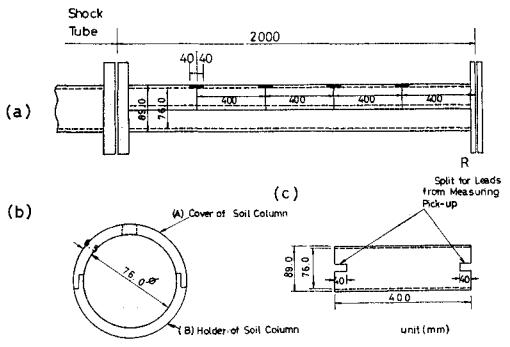

Fig. 8 Testing apparatus; (a) confining tube of soil specimen, (b) cross section and (c) segment.

In order to eliminate the friction between the soil and the inside wall of the confining tube, teflon sheets with silicon glease are used through the experiment.

b) Experimental Procedure

1) Soil

Sandy loam (G_s=2.66) was selected as the soil sample in this study on stress wave propagation. It was sieved by 2 mm mesh and a part which passed through it was used. The mean diameter is about 0.3 mm and the uniformity coefficient is 22.5. The optimum moisture content is about 12%, which gives the maximum dry density of 1.9 g/cm^3.

2) Test series

The characteristics of stress wave in soil depend upon various physical and mechanical properties of soil; for example, type of soil, magnitude of loading, soil confinement, density, moisture content and so on[9]. In order to clarify problems concerning stress wave propagation, therefore, one has to investigate them by taking every factors mentioned above into account. In the present study the authors selected a physical variable; the bulk density and a mechanical one;

Table 1 Test series.

(a) Test Series A

Supplied Pressure in High Pressure Chamber

Density		I	II	III	IV	V	VI	VII
		3 kg/cm^2	6 kg/cm^2	8 kg/cm^2	10 kg/cm^2	12 kg/cm^2	14 kg/cm^2	16 kg/cm^2
a	1.7 g/cm^3	A-I-a	A-II-a	A-III-a	A-IV-a	A-V-a	—	—
b	1.8 g/cm^3	A-I-b	A-II-b	A-III-b	A-IV-b	A-V-b	A-VI-b	A-VII-b
c	1.9 g/cm^3	A-I-c	A-II-c	A-III-c	A-IV-c	A-V-c	A-VI-c	A-VII-c

(b) Test Series B

Supplied Pressure in High Pressure Chamber

Density		I	II	III	IV	V	VI	VII
		3 kg/cm^2	6 kg/cm^2	8 kg/cm^2	10 kg/cm^2	12 kg/cm^2	14 kg/cm^2	16 kg/cm^2
a	1.7 g/cm^3	B-I-a	B-II-a	B-III-a	B-IV-a	B-V-a	—	—
b	1.8 g/cm^3	B-I-b	B-II-b	B-III-b	B-IV-b	B-V-b	B-VI-b	B-VII-b
c	1.9 g/cm^3	B-I-c	B-II-c	B-III-c	B-IV-c	B-V-c	B-VI-c	B-VII-c

the magnitude of applied pressure at the surface of the soil column. The moisture content of soil is also one of the most important factors which influence the characteristics of stress wave. The investigation over a wide range of moisture content is required. In this study, however, the moisture content was kept constant, *i.e.*, 5 to 7% which was relatively small compared with the optimum.

The experiments for the stress wave propagation was performed for three kinds of bulk density (1.7 g/cm^3, 1.8 g/cm^3 and 1.9 g/cm^3) and seven levels of applied pressure. It has been mentioned above that the obtained shock pressure at the end of the shock tube can be roughly predicted by the supplied pressure in the high pressure chamber. In the present study, therefore, the test series were planned as shown in Table 1 with the combination of the bulk density and the supplied high pressure. The test series A concerns with observation of peak stress, rise time and velocity of stress waves by detecting from soil stress transducers at several points in the soil column. The series B is for the investigation of stress-strain relationships of the soil during stress wave propagation by using stress transducers and strain-meter.

3) Preparation of soil samples

For the preparation of soil samples in this experiment a special split mold with an inside diameter of 7.45 cm and a height of 40 cm was used. The inside surface of the mold was made very smoothly. In the mold a sandy loam was compacted by means of a 2.5 kg rammer with 30 cm free-fall in six layers with five blows per layer in the case of bulk density $\gamma=1.7$ g/cm^3, in six layers with ten blows in $\gamma=1.8$ g/cm^3 and in seven layers with fifteen blows in $\gamma=1.9$ g/cm^3.

The void ratio e is more convenient to represent the degree of soil compaction than the bulk density γ. Throughout all test series, the void ratio was in the range of $e=0.66-0.67$ in the case of the bulk density $\gamma=1.7$ g/cm^3, $e=0.56-0.58$ in $\gamma=1.8$ g/cm^3 and $e=0.47-0.49$ in $\gamma=1.9$ g/cm^3.

4) Setting up soil samples

In the experimental study for the stress wave propagation in confined soils, the friction forces between the inside wall of confining tube and the surface of soil specimen should be taken away. However, it is actually impossible to completely reduce the friction. In order to minimize the friction as much as possible and, at the same time, to keep the condition of lateral confinement to the soil, the compacted soil specimens were rolled by two teflon sheets of 0.1 mm and 0.4 mm thickness. This procedure gives the best result in reducing the friction.

Five pieces of specimen prepared by the mold were required to be set in the confining tube to fill it up. In this case, it is with no doubt that great attention should be paid not to break it and not to create discontinuities at the joints of specimens. By this way the two-meter long confined soil column was made up as shown in Photo. 3. Then it is covered by the remainder of the half of the tube.

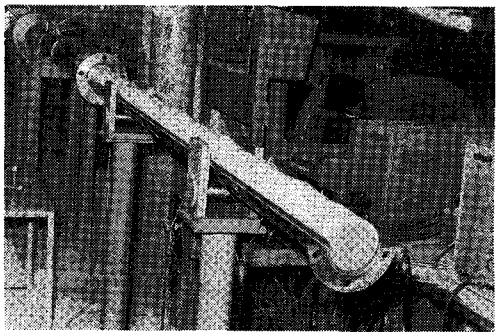

Photo. 3 Soil column rolled by two teflon sheets.

5) Measuring system

The schematic diagram of the measuring system used in this experiment is shown in Fig. 9. It consists of measuring pick-ups, amplifiers and synchroscopes. The phenomena are recorded by polaroid cameras.

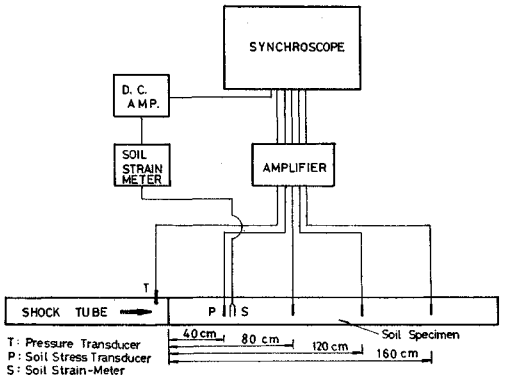

Fig. 9 Schematic diagram of the measuring system used.

Four soil stress transducers and a strain-meter were embedded in the soil column at intervals of 40 cm. The phenomena were observed at the same time by the four-channel and two-channel synchroscopes. These were initially triggered by

the top soil stress transducer which was the nearest from the impact end of the soil column, and by the pressure transducer, respectively.

(2) Soil Stress Transducer

a) General

With the progress of soil mechanics it has been required so much to know the state of stresses in soil. In spite of recent development of pressure transducers, there remain many uncertainties in their use to measure the true stress in soil. The difficulty is said to be caused by an arching effect due to the different rigidity between the soil and the pick-ups[10].

These phenomena are caused by the characteristics of soil. When a transducer is used in a liquid or gas, these would vanish. Before using soil stress transducers, we have to carry out the calibration test under the same condition as actual one[11].

b) Calibration

One of four stress transducers used in this study is shown in Photo. 4, which was 2.5 cm in diameter and 0.5 cm in thickness. Since the transducer is made of semi-conductive strain gauge, it has a relatively high sensitivity. The characteristics of this transducer are shown in Table 2.

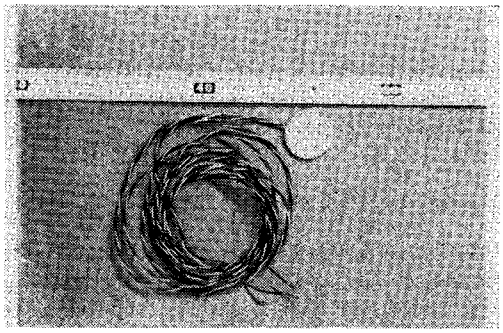

Photo. 4 Soil stress transducer.

Table 2 Characteristics of soil stress transducer used.

Nominal capacity	10 kg/cm^2
Overload to	15 kg/cm^2
Output at nominal capacity	1 905×10^{-6}
Overall accuracy	1%
Bridge input imp.	120 Ohms
Bridge output imp.	120 Ohms
Temperature range	40°C

Three kinds of calibration test were carried out, by air pressure, by oil pressure and by soil pressure. The calibration curves for the former two are almost equal to each other. The manner of calibration test in soil is shown in Fig. 10. The soil used in this calibration was the sandy loam for the following wave propagation tests. The soil was packed till four-fifth height in the circular cell of 12 cm inside diameter and 20 cm in height. The soil stress transducer was embedded at the depth of 1–2 cm. The leading wires were taken out from the hole on side wall and connected with the indicator. A rubber sheet was covered on the soil surface, then the air pressure controlled by the regulator was applied on the soil surface.

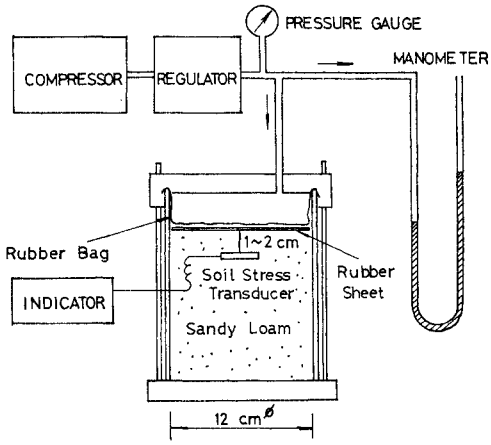

Fig. 10 Manner of calibration test in soil.

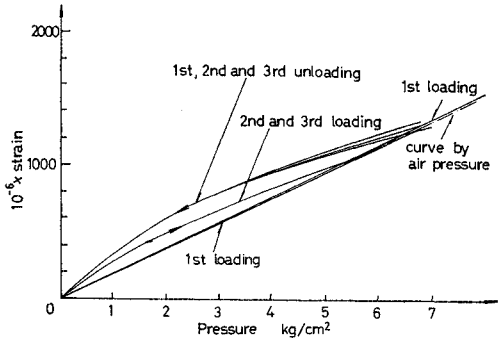

Fig. 11 Typical calibration curves of soil stress transducer.

Fig. 11 indicates the typical calibration curves obtained by three cycles of loading and unloading. In the first loading the output (μ-strain) of the indicator increased linearly with increase in the pressure. It almost agreed with the result

obtained by application of direct air pressure. However, the unloading curve is different from it. During one cycle of pressure, a large amount of hysteresis loop appeared. In the second and third loading, on the other hand, the curves seemed to approach the first unloading curves, while the unloading curves almost equaled to the first one. These tendencies could be seen in other three transducers.

c) Embedding of Soil Stress Transducers

In the experiment for stress wave propagation, a soil stress transducer was embedded at the centre of cross section of the sample when preparing soil sample in the mold. The place of embedding was at the depth of 4 cm from the top of the mold. After embedding the transducer, compaction was continued by the same way as mentioned above. In this case attention was required not to break the pick-ups.

(3) Condenser-type Soil Strain-Meter

a) General

It is of great importance in the field of soil mechanics to measure exactly local strains as well as local stresses in soil without disturbing it. As mentioned above, since soil stress gauge instrumentations have been developed so much, it is fairly easy to measure stresses in natural state of the ground. An appropriate instrumentation to measure local strains in soil has not been established in this country. Especially, it has been impossible to measure dynamic strains in soil.

In the United States soil strain gauge instrumentation has been developed by IITRI to measure transient soil deformations in both laboratory and field applications[12]. This strain sensor consists of two flat-coil disks which are embedded in soil in near parallel and in concentric orientation without physical connection between them. The remainder of the gauge hardware consists of a second set of coil disks, identical to those used as the strain sensor, and specially designed electronic driving, amplifying, balancing and recording circuitly. Soil deformations are measured by the resulting changes in the spacing of embedded coils which are sensed as changes in the mutual inductance of the coils. This strain sensor is used in many kinds of soil testing, for example, triaxial compression tests, wave propagation studies in soil and so on[4),5)].

b) Principle of Strain-Meter

The authors devised a condenser-type soil strain-meter in order to measure the one-dimensional soil deformations during stress wave propagation. This type of strain-meter has been used in air[13], but never used in soil as a dielectric substance. This strain-meter consists of two flat electrode plates embedded in soil in parallel and in concentric orientation. Soil deformations are measured by the resulting changes in the spacing of embedded two plates which are sensed as changes in the electrostatic capacity of them.

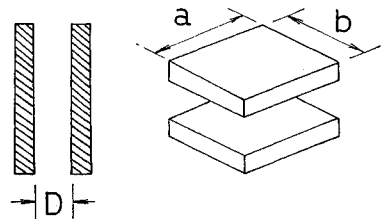

Fig. 12 Two conductors in parallel.

When two conductors are placed in parallel as shown in Fig. 12, the resulting electrostatic capacity is given by

$$C=\frac{A\varepsilon_0\varepsilon_s}{D}=8.885\times10^{-12}\times\frac{A\varepsilon_s}{D}\quad[\mathrm{F}]$$

$$=8.885\times\frac{A\varepsilon_s}{D}\quad[\mathrm{pF}]\cdots(12)$$

where, A denotes the cross sectional area ($a\times b$ (m^2)) of the conductor, D the spacing of two conductors (m), ε_0 the dielectric constant and ε_s the specific dielectric constant. Eq. (12) implies that if ε_s is assumed to be constant through testing, the variation in the spacing ΔD of two conductors results in the change in capacity ΔC:

$$\Delta C=\frac{\partial C}{\partial D}=8.885\times\frac{A\varepsilon_s}{D^2}\Delta D\quad[\mathrm{pF}]\cdots(13)$$

The strain-meter consists of the bridge circuit indicated in Fig. 13, where C_3 and C_4 denote the fixed condensers, C_2 the variable condenser, C_a the measuring condenser embedded in soil and

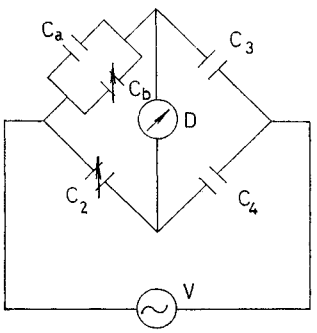

Fig. 13 Bridge circuit in the strain-meter.

C_b the variable condenser to control an initial capacity in the calibration test equally to the initial capacity in the experiment.

e) Calibration

The apparatus of soil strain-meter, as shown in Photo. 5, consists of a meter MD-12, a probe MDG-643, a variable condenser for calibration test and two electrode plates embedded in soil. The size, shape and material of the electrode plates are optional. In this study the rectangular copper plates (2.5 cm × 1.5 cm) were used. Since they were coated by enamel, this soil strain-meter could be used even in wet soils.

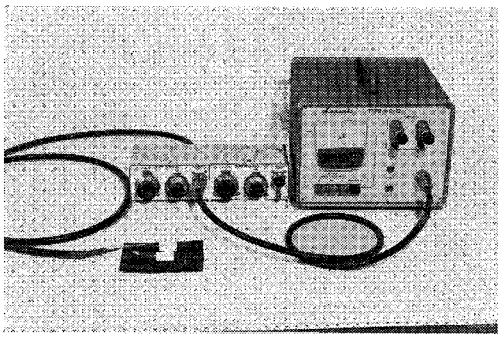

Photo. 5 Condenser-type soil strain-meter.

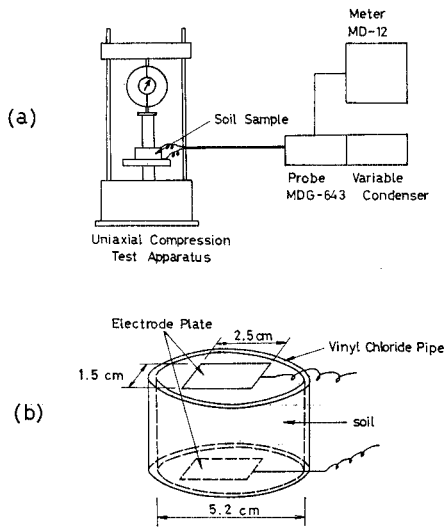

Fig. 14 Calibration of soil strain-meter; (a) manner of calibration and (b) description of soil sample.

Fig. 14(a) indicates the manner of calibration and (b) is the description of soil sample (sandy loam). The sample was packed in a ring made of vinyl-chloride of which inside diameter and height were 5.2 cm and 2.0 cm, respectively. As shown in Fig. 14(b) two electrode plates were put on the upper and lower surfaces in concentric orientation so that the initial spacing between two plates was 2.0 cm. After setting up the apparatus and balancing the bridge circuit in the prove MDG-643, soil sample was compressed by means of uniaxial compression apparatus and, at the same time, the resulting electric current was read.

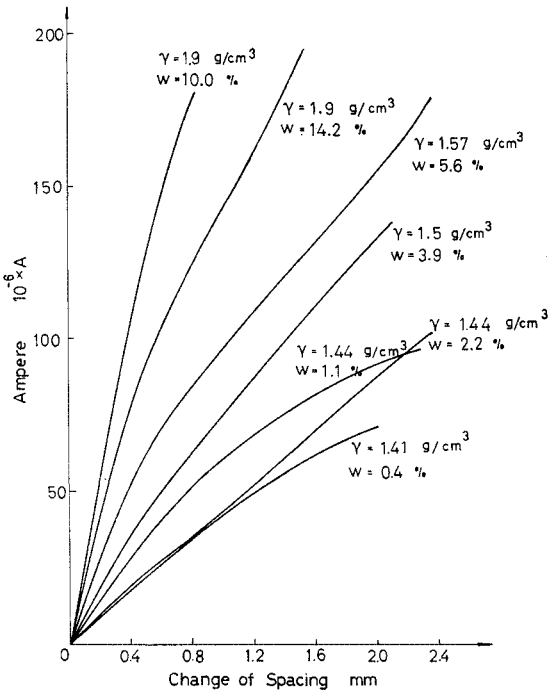

Fig. 15 Typical calibration curves of soil strain-meter.

A typical example of the calibration curves is given in Fig. 15. It is found from this figure that each curve is smooth but varies with the water content w and the bulk density γ of the soil sample. The slope of the curve becomes steeper with increase in γ.

4. EXPERIMENTAL RESULTS

(1) Soil Surface Pressure

The soil surface pressure was applied by the shock tube and measured by the pressure transducer which was equipped at the end of the low pressure chamber. Since the distance between the transducer and the soil surface is as small

as about 6 cm, the pressure wave on the pressure transducer may be regarded as the applied soil surface pressure.

In the preceding section the manner has been described about the shock pressure obtained at the end of tube by covering the end with a steel plate. However, provided the end is deformable, for example, the soil in this study, the obtained pressure form is different from that. Two typical wave forms with respect to time are illustrated in Fig. 16. Fig. 16(a) is the wave form for relatively low pressure, and (b) for relatively high pressure. In the former case, the incident shock pressure coincides with the peak pressure since the reflected pressure at the soil surface is small. In the latter case, the peak pressure arises behind the incident shock pressure, since the reflected pressure is large.

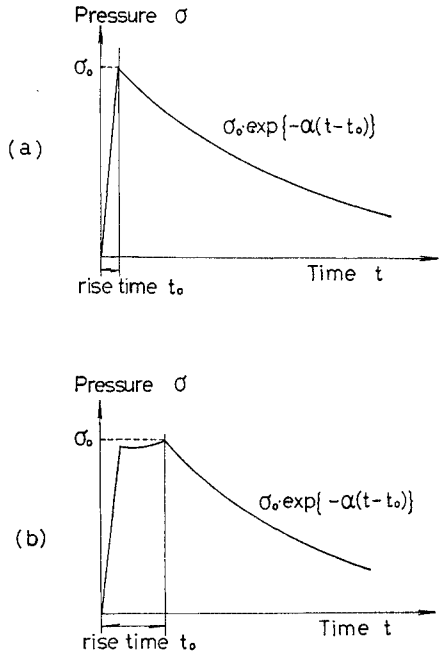

Fig. 16 Two typical wave forms with respect to time; (a) wave form for relatively low pressure and (b) for relatively high pressure.

The obtained surface pressure has a rise time of 0.6 msec−1.4 msec and decays exponentially after peak. Therefore, the semi-logarithmic plotting of it indicates approximately straight line as illustrated in Fig. 17. We express the surface pressure as:

$$\sigma(0, t)=\sigma_0 \exp(-\alpha t) \qquad \cdots\cdots(14)$$

where, σ denotes the surface pressure, σ_0 the peak pressure, α the decaying parameter and t the time after peak (in sec). Fig. 18 shows the correlation between the decaying parameter and the surface pressure.

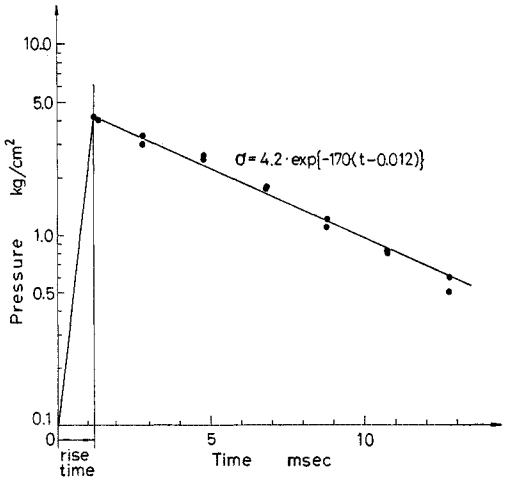

Fig. 17 Semi-logarithmic plotting of soil surface pressure.

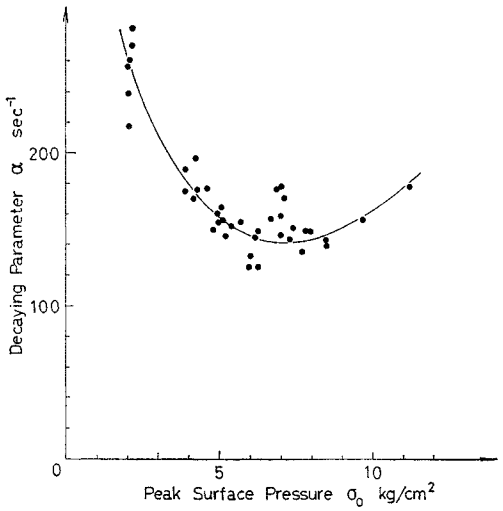

Fig. 18 Correlation between the decaying parameter and the surface pressure.

(2) Wave Velocity

Fig. 19 shows schematically four wave forms observed on the synchroscope. The velocity of wave propagation is determined for each test series by plotting the time of wave arrival at each soil stress transducer as a function of its position.

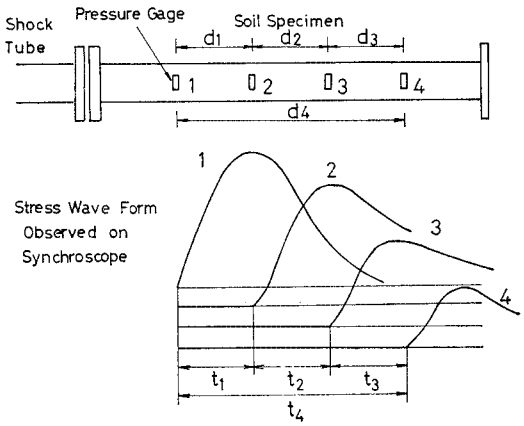

Fig. 19 Four wave forms observed on the synchroscope.

Throughout all experimental data it can be seen that the wave velocity varies with the void ratio, the pressure level and the repetitive loading. In the series of test the load is applied three times in order to observe the effect of repetitive loading on the behavior of wave propagation. From the experimental result one can notice that the rate of increase in the velocity due to repetitive loading becomes larger in the case of lower void ratio. In the case of higher void ratio, on the other hand, there exists no difference between the second and the third loading, and the increase in the velocity with the surface pressure cannot be seen even in repetitive loading.

According to the detailed examination of experimental data, the propagating velocity of stress wave tends to attenuate with depth. This phenomenon should be considered to be caused by the non-linearity in stress-strain relationships and the dissipative mechanism of the soil tested. That is, the peak stress at the surface gradually attenuates with the stress wave propagating through the soil. Consequently, the wave will attenuate with depth. In order to quantitatively understand these phenomena, it is suitable to obtain the correlation between the local velocity and the carrying stress in the soil. Fig. 20 indicates this relationship, showing the following remarkable tendencies, although the results involve scattering about 15%:

1) The wave velocity increases with increase in the carrying stress level for certain range of void ratio. For the larger void ratio, however, the velocity does not change in this experiment.
2) The wave velocity at a same carrying stress level increases with decrease in the void ratio.

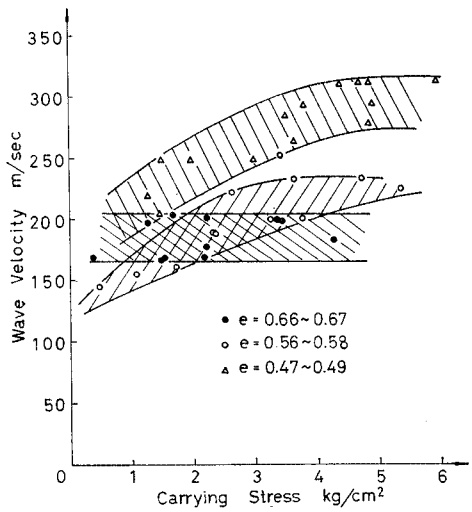

Fig. 20 Correlation between the local velocity and the carrying stress in soil.

Hardin and Richart[14] summarized the experimental results from many investigators for variation in seismic velocity (compressive wave and shear wave) with confining pressure. The plotting on logarithmic scale is shown in Fig. 21, in

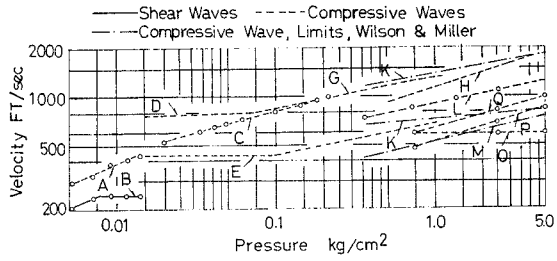

Fig. 21 Variation in seismic velocity with confining pressure (after Hardin and Richart).

which the authors' results given in Fig. 20 are also denoted by the lines O, P and Q by considering the acting pressure as the confining pressure. One can see from this figure that the logarithm of wave velocity increases linearly with the logarithm of pressure.

(3) Stress Wave Pattern

a) Peak Stress Attenuation

The variation of peak stress and rise time along the specimen is an important phenomenon in materials exhibiting the damping effect of energy, such as soil[15]. Fig. 22 shows an example of re-

cords on the synchroscope, indicating the wave pattern measured at various depths in the soil specimen, together with the surface pressure.

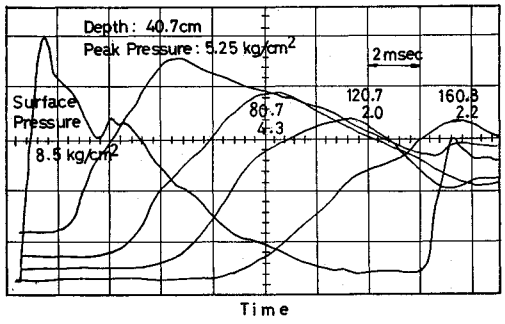

Fig. 22 Example of records on the synchroscope.

Dimensionless stress Σ' is defined by stress σ in the soil divided by the peak surface pressure. Now on, we use "stress" as the dimensionless stress, unless specified.

It is examined how the applied surface pressure influences on the attenuation of peak stress. Selig and Vey[16] conducted stress wave propagation tests by using the confined Ottawa sand specimens having 64 in. (153.6 cm) in length. They obtained the results of attenuation of peak stress under various shock pressures and confining pressures, in the range of 0.35 kg/cm² to 1.6 kg/cm². They concluded that attenuation increased at a successively greater rate as the peak applied pressure increased and that attenuation approached zero as the peak applied pressure approached zero, *i.e.*, as the wave propagation approached the elastic state. In the authors' experimental results, however, attenuations at a given void ratio are almost constant throughout all applied pressure levels used. From this one can see that the attenuation at a given bulk density is approximately constant and the peak stress attenuates exponentially. By taking this fact into account and adopting the average value in all results, an explicit tendency is found out that the attenuation increases with increase in the void ratio. It is shown in Fig. 23 and may be of great importance to understand the wave propagation mechanism and the damping effect of soil.

Replotting this correlation on a semi-logarithmic paper, as shown in Fig. 24, the peak stress decreases approximately linearly with depth. As-

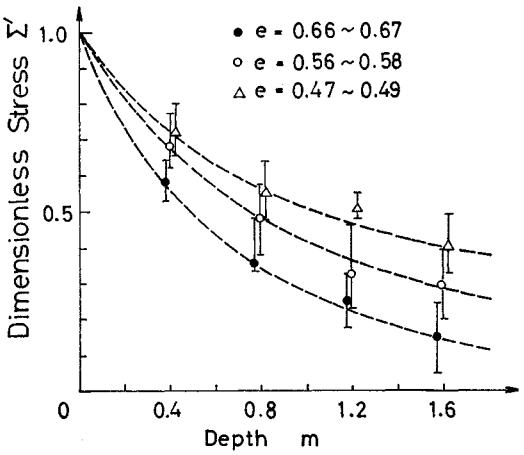

Fig. 23 Peak stress attenuation.

suming above correlations to be linear, the attenuation of peak stress along the specimen is represented by the following equation:

$$\Sigma' = \exp(-\delta x) \qquad \cdots\cdots(15)$$

where, Σ' denotes the dimensionless stress, δ the attenuation constant and x the depth (m). The attenuation constants determined from Fig. 24 are as follows:

$\delta = 1.22$ for the case of $e = 0.66 - 0.67$,

$\delta = 0.93$ for the case of $e = 0.56 - 0.58$ and

$\delta = 0.63$ for the case of $e = 0.47 - 0.49$.

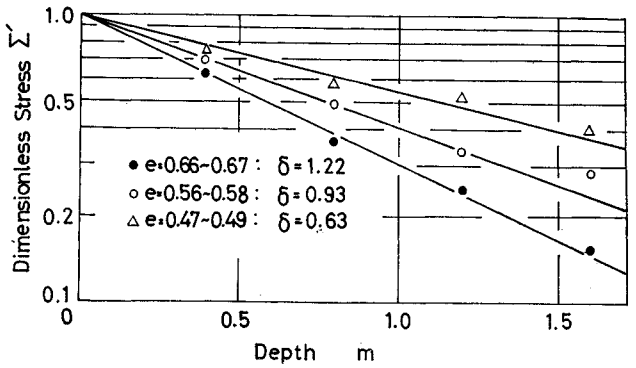

Fig. 24 Semi-logarithmic plotting of peak stress attenuation.

Fig. 25 shows the linear relationships on the logarithmic paper between the void ratio e and the attenuation constant δ determined from Fig. 24.

b) Rise Time of Stress Wave

Another measure to represent collapse of wave is the rise time. Dimensionless rise time T is defined as:

$$T=\frac{t_x}{t_0} \qquad \cdots\cdots(16)$$

where, t_0 denotes the rise time of stress wave obtained from the transducer at the depth of 40 cm and t_x the rise time at a certain depth.

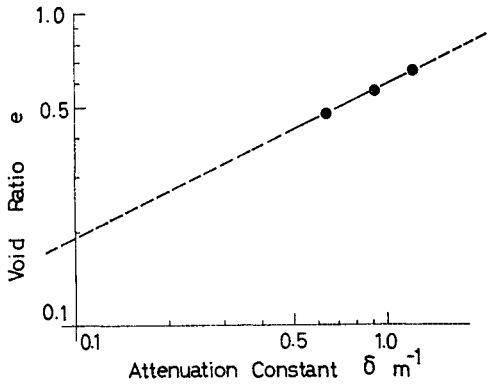

Fig. 25 Relationship between the void ratio and the attenuation constant.

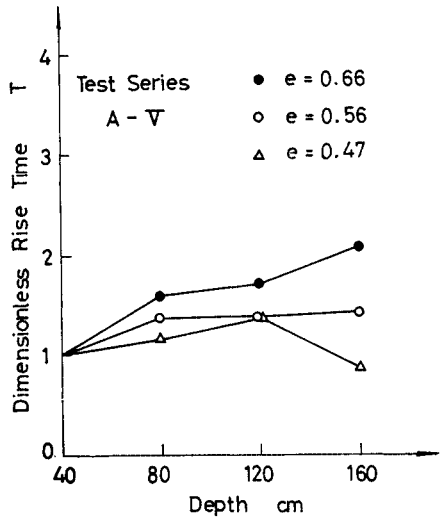

Fig. 26 Variation in rise time along the specimen.

Fig. 26 indicates an example showing the variation in rise time along the specimen at a given applied surface pressure. In general the rise time increases with depth and with decrease in the void ratio. In some cases one can see that the rise time decreases at the reflection end of soil specimen, especially for lower void ratio (e=0.47–0.49) and high pressure level. This may be caused by the superposition of the reflected wave on the incident wave.

(4) Dynamic Stress-Strain Relationships

In the present series of shock tube test, a pair of soil stress transducer and soil strain-meter was embedded in the specimen. A typical record of the synchroscopic trace is shown in Photo. 6. The calibration tests for strain-meter were carried out after every experiment completed. By using the stress-time and the strain-time correlations at the depth of 40 cm, dynamic stress-strain relationships were obtained by replotting stress and strain values corresponding to the same instant of time.

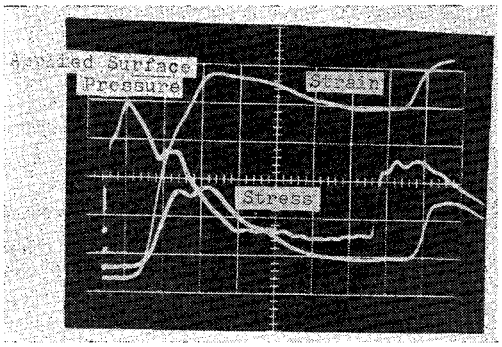

Photo. 6 Typical record of synchroscopic trace.

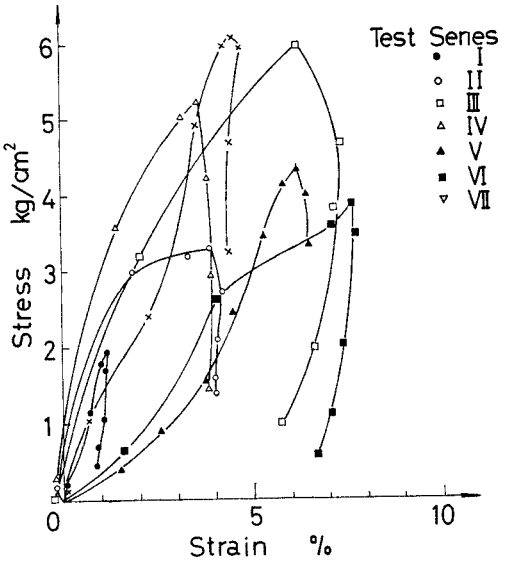

Fig. 27 Dynamic stress-strain relationships.

An example of the obtained dynamic stress-strain relationships for medium soil density is shown in Fig. 27. It is perhaps worth mention-

ing that, for higher void ratio (e=0.66−0.67), the shape of stress-strain curves is of softening type without regard to the magnitude of stress. For medium (e=0.56−0.58) and lower void ratios (e=0.47−0.49), on the other hand, the curves tend to be of locking type or S-shaped, especially for relatively high pressure level. Initial tangent of the stress-strain curves seems to increase with decrease in void ratio.

5. DISCUSSIONS AND CONCLUSIONS

Throughout the experimental investigation descrived in this study, some important conclusions can be obtained and summarized with some discussions as follows.

(1) The shock tube used in the present study is appropriate as a dynamic loading apparatus for confined soils. It has following main merits:
   a) It is easy to control the magnitude of a shock pressure.
   b) The wave form of shock pressure obtained has an acute wave front and a decaying part which can be expressed by $\exp(-\alpha t)$. This is very suitable for analytical consideration[17].

(2) The condenser-type strain-meter developed in this study is useful to measure local strains in soil without regard to static or dynamic strain. There remain some problems about its usage to be solved, however, for example, to minimize disturbance of soil when installing it into the specimen and to develop more refined calibration procedure.

(3) The velocity of wave front extremely depends upon the soil density, the magnitude of surface pressure and the repetitive loading. It increases with increase in them. There exists similar tendency as previous studies that the logarithmic plotting of wave velocity indicates linear increase with the carrying pressure of stress wave.

(4) The attenuation of peak stress during the wave propagation in confined sandy loam indicates a pattern of exponential decay. It depends mainly on the void ratio, but neither on the applied pressure level nor on repetitive loading.

(5) The rise time of stress wave increases with depth and with decrease in void ratio of soil specimen. The degree of variation in rise time along the depth of specimen is 1−1.5 times the basic rise time.

(6) The shape of dynamic stress-strain curves for higher void ratio is of softening type without regard to the magnitude of stress. For medium and lower void ratios, on the other hand, the curves tend to be of locking type or S-shaped, especially for relatively high pressure level.

The authors would appreciate Professor G. Kamimoto in the Department of Aeronautic Engineering, Kyoto University, who kindly advised them in designing the shock tube apparatus. Thanks are also due to Dr. T. Adachi, Colleague in the Soil Mechanics Laboratory in Kyoto University, for his close participation in instrumentation works.

REFERENCES

1) Akai, K., M. Tokuda and T. Kiuchi: Experimental Study on the Propagation of Stress Wave in Cohesive Soils, Proc. JSCE, No. 161, 1969, pp. 59-67.
2) Akai, K. and M. Hori: Basic Study on the Dynamic Soil-Structure Interaction, Proc. JSCE, No. 173, 1970, pp. 61-78.
3) Glass, I. I. and J. G. Hall: Shock Tubes (Handbook of Supersonic Aerodynamics, Section 18), NAVORD Rep. 1488, Vol. 6, 1959, pp. 1-2.
4) Vey, E. and L. V. Strauss: Stress-Strain Relationships in Clay Due to Propagating Stress Waves, Proc. Int. Symp. Wave Propagation and Dynamic Properties of Earth Materials, Univ. New Mexico, 1967, pp. 575-586.
5) Hampton, D. and R. A. Wetzel: Stress Wave Propagation in Confined Soils, Proc. Int. Symp. Wave Propagation and Dynamic Properties of Earth Materials, Univ. New Mexico, 1967, pp. 433-442.
6) Kamimoto, G.: Shock Tube Theory (Preprint), 1965, pp. 1-31 (in Japanese).
7) Kamimoto, G.: Shock Tunnel Technology J. JSAS, Vol. 11, No. 117, 1963, pp. 310-317 (in Japanese).
8) Whitman, R. V.: Discussion on "Theory Compared with Experiments on Sand Colums" by B. R. Parkin, Trans. ASCE, Vol. 127, Part 1, 1962, pp. 1308-1317.
9) Kondner, R. L.: Stress Wave Propagation Phenomena in Terms of Dynamic Response Spectra, Proc. Int. Symp. Wave Propagation and Dynamic Properties of Earth Materials, Univ. New Mexico, 1967, pp. 483-490.
10) Abbott, P. A., K. B. Shimmons, C. M. Reiff and S. Mitchell: Recent Soil Stress Gage Research, Proc. Int. Symp. Wave Propagation and Dynamic Properties of Earth Ma-

terials, Univ. New Mexico, 1967, pp. 221-238.
11) Ichihara, M. and K. Furukawa: Experimental Studies on Calibration of Earth Pressure Cells, Trans. JSCE, No. 135, 1969, pp. 8-15 (in Japanese).
12) Truesdale, W. B. and R. B. Schwab: Soil Strain Gage Instrumentation, Proc. Int. Symp. Wave Propagation and Dynamic Properties of Earth Materials, Univ. New Mexico, 1967, pp. 931-941.
13) Takenaka, J.: Measurements of Stress, Asakura Book Co., 1964, pp. 261-285 (in Japanese).
14) Hardin, B. O. and F. E. Richart: Elastic Wave Velocities in Granular Soils, Proc. ASCE, Vol. 89, SM 1, 1963, pp. 33-65.
15) Akai, K. and M. Hori: A Viscoelastic Approach to the Problem of Stress Wave Propagation in Cohesive Soils, Proc. JSCE, No. 185, 1971, pp. 95-103.
16) Selig, E. T. and E. E. Vey: Shock Induced Stress Wave Propagation in Sand, Proc. ASCE, Vol. 91, SM 3, 1965, pp. 19-49.
17) Akai, K. and M. Hori: Analytical Study on Stress Wave Propagation in Viscoelastic Materials Subjected to Spike Pulse, Proc. JSCE, No. 195, 1971, pp. 91-98.

(*Received Sept. 10, 1971*)

地下水の追跡に

MITY
蛍光光度計

■用　途

○地下水の研究

○ダムの漏水、トンネル及農薬用水の漏水

○地辷対策

○岩盤の亀裂の水の関連性研究

■特　長

現場に持込み可能

小型（26cm×23cm×22cm）

■納入実績

大学・官庁研究所・各府県砂防，
耕地，農地建設，治山，其他

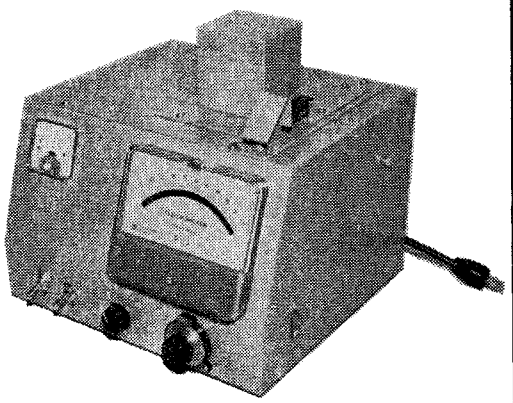

東京測器製作所

〒140
東京都品川区西大井1丁目5番9号
電話　東京　03〈772〉6017

土木関係計測器

及各種土質試験機
専門メーカー

1）　地すべり関係
2）　井筒，せん函又は擁壁関係
　　及びコンクリートダム関係
3）　トンネル関係
4）　Open cut又は地下鉄工事関係
5）　シールド関係
6）　梁堤ならびにアースダム関係
7）　軟弱地盤関係
8）　坑，地中壁，構造物の変状関係
9）　地震関係
10）　道路関係
11）　各種土質試験機関係
12）　各種公害関係

差動トランス型間隙水圧計

差動トランス型土圧計

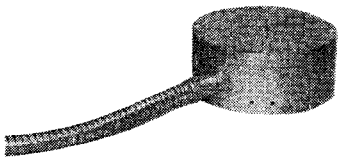

営業品目
坂田式各種土圧計／加速度計／変位計／歪計／傾斜計／間隙水圧計／鉄筋計／沈下計各種／パイプひずみ傾斜計／水平振子傾斜計／地すべり記録器各種／地下水検層器／水位警報装置／地すべり崩雪検知装置／シールド工法進路補正装置／コンクリート直視歪計／支柱式ロードセル／バーニヤスケール各種／腐蝕率計／振動計／自記式三軸圧縮試験機／振動三軸試験機／走行車両重量選別積算装置／道路試験車装置／指示騒音計外公害関係計測器／その他電気応用計測器／等の製造・販売・修理／

坂田電機株式会社

営業所
工　場　東京都保谷市柳沢2丁目17番20号
電　話　0424－62－6811代表　〒188

昭和三十七年五月二十八日　第三種郵便物認可
昭和四十七年四月十五日　印刷（毎月一回）
昭和四十七年四月二十日　発行（二十日発行）

土木学会論文報告集　第200号

土木計測用 ひずみゲージ式 変換器

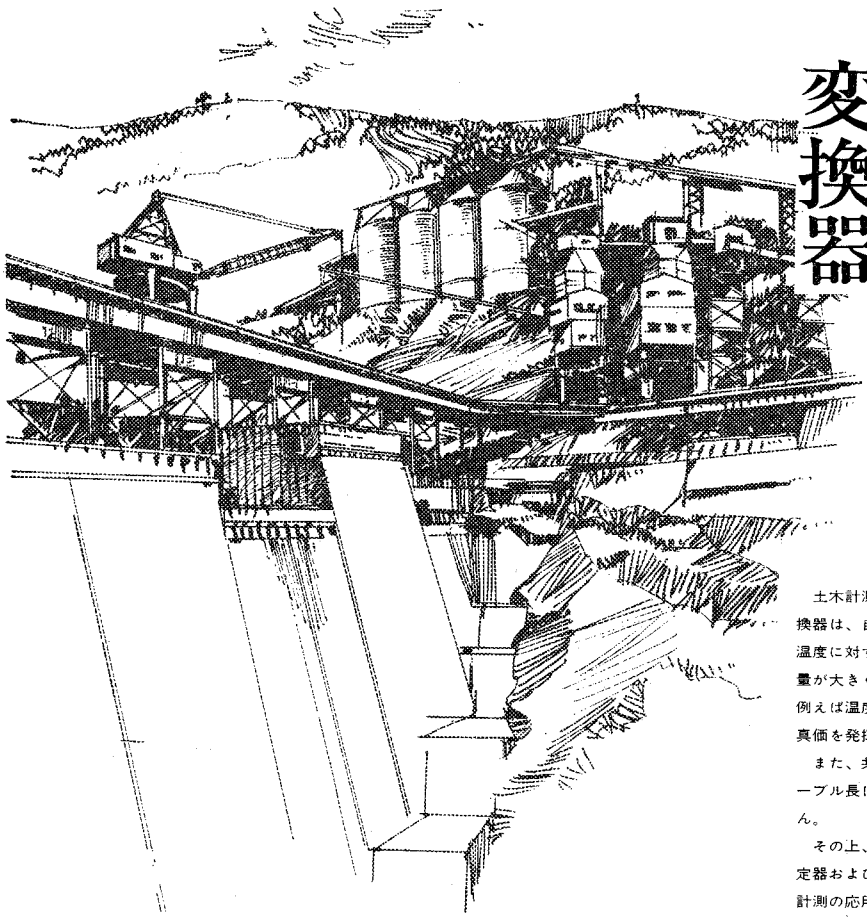

土木計測用に開発されたひずみゲージ式変換器は、自己温度補償の原理を取り入れて、温度に対する補正が不要になりました。補正量が大きく真値のつかみにくい場での計測、例えば温度変化の大きい場などで使用すれば、真価を発揮します。

また、共和独特の指示器の採用により、ケーブル長は5kmまで感度に全く影響ありません。

その上、市販されているすべてのひずみ測定器およびその周辺器が使用できますので、計測の応用範囲が広がり便利になりました。

特　長

- ●温度補正はいりません
- ●ケーブル抵抗の補正は5kmまで全く不要
- ●あらゆるひずみ測定器に接続できる
- ●小型の構造物にも使える
- ●耐環境性にすぐれ、信頼性が高い

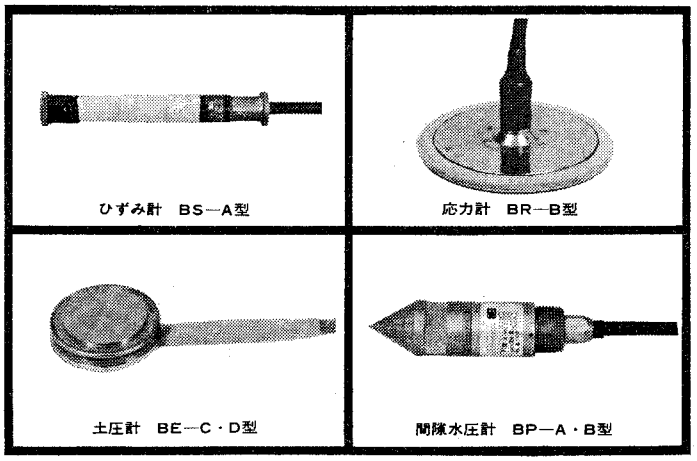

ひずみ計　BS—A型

応力計　BR—B型

土圧計　BE—C・D型

間隙水圧計　BP—A・B型

種　類

品　名	型　式　名	容　量
ひずみ型	BS－A型	±500×10⁻⁶ひずみ
応　力　計	BR－B型	20, 50, 100kg/cm²
間隙水圧計	BP－A型	2,5,10,20kg/cm²
	BP－B型	2,5,10,20kg/cm²
土　圧　計	BE－B型	2,5,10kg/cm²
	BE－C型	
	BE－D型	
	BE－E型	2,5,10,20kg/cm²
	BE－F型	
変位変換器	BCD　型	±5mm

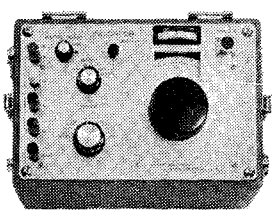

専用指示器　BM－12A

●カタログお送りいたします。
誌名記入のうえ広報係まで

土木計測器の専門メーカー

共和電業

本社・工場　東京都調布市下布田1219
電　　話　東京調布0424－83－5101

営業所／東京・大阪・名古屋・福岡・広島・札幌　出張所／水戸

定価四五〇円